https://dx.doi.org/10.1016/j.cclet.2023.108709
This is the Pre-Published Version.

Development and application of photocatalytic coating for roadside NOx mitigation in Hong Kong

Xinwei Li[a], Pengge Wang[b], Shuwen Han[a], Yu Huang[b,*], Wingkei Ho[c], Steven Sai Hang Ho[d], Shun-cheng Lee[a,*], Meng Wang[a]

[a] Department of Civil and Environmental Engineering, The Hong Kong Polytechnic University, Hong Kong, China

[b] State Key Laboratory of Loess and Quaternary Geology (SKLLQG) and Key Laboratory of Aerosol Chemistry and Physics, Institute of Earth Environment, Chinese Academy of Sciences, Xi'an 710061, China

[c] Department of Science and Environmental Studies, The Education University of Hong Kong, Hong Kong, China

[d] Division of Atmospheric Sciences, Desert Research Institute, Reno, NV 89512, United States

[*] Corresponding Authors: huangyu@ieecas.cn (Y. Huang), shun-cheng.lee@polyu.edu.hk (S. Lee).

Graphical Abstract

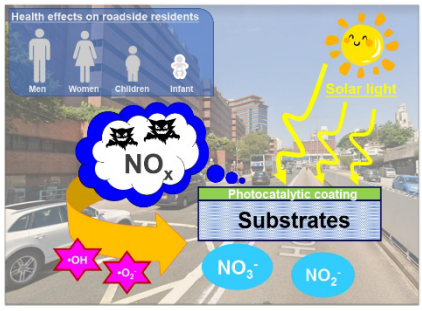

This work demonstrates the feasibility of air pollution control measures for the local roadside NO_x using photocatalytic technology, offering promising health benefits with environmental remediation.

© 2023. This manuscript version is made available under the CC-BY-NC-ND 4.0 license http://creativecommons.org/licenses/by-nc-nd/4.0/.

Abstract

A facile chemical method for the development of photocatalytic coating products was proposed based on practical application perspective for the Hong Kong roadside nitrogen oxides (NO_x) mitigation. TiO_2-based photocatalytic coating PC-C film with crystallized size of around 5–6 nm was synthesized with the peptization of H_2O_2. The PC-C coating possesses a super-hydrophilicity surface and is proven to have a NO_x degradation rate of 46.8% with an optimum pH level of 7. In addition, the PC-C coating presents a promising photocatalytic NO_x degradation compared with other commercially available coating products and P25 when applied on two building materials of Poly-methyl methacrylate (PMMA) and concrete surface. A weather resistance simulation and a 180-day on-site field trial were carried out the attenuation effects of photocatalytic coating applied in outdoor exposure. Based on epidemiological estimation and field investigation, hospital admissions for respiratory diseases (HARD) and mortality cases (MC) could be reduced with the application of PC-C coating along the street canyon. This work demonstrates the feasibility of air pollution control measures for the local roadside NO_x using photocatalytic technology, offering promising health benefits with environmental remediation.

Keywords

Photocatalysis; Coating; NO_x mitigation; Hong Kong; Roadside

Nitrogen oxides (NO_x, *i.e.*, NO + NO_2), as notorious atmospheric pollutants, not only promote the formation of ozone and secondary aerosols [1, 2], but also exhibit adverse health effects on human with increasing respiratory deaths and lung cancer deaths [3-5]. As a densely populated urban metropolis, traffic-related emissions contributed to the majority of Hong Kong's NO_x pollution [6, 7]. To improve air quality, the Hong Kong Environmental Protection Department (HKEPD) has implemented a series of emission control measures successfully contributing to the steady decline in air pollution levels in recent years [7-9]. However, challenges still exist, that is, the roadside NO_2 level still exceeds the Hong Kong Air Quality Objectives (AQO) and World Health Organization (WHO) global Air Quality Guidelines (AQG) [10, 11]. Thus, innovative air pollution control technologies should be implemented at the same time to supplement the current emission control technologies.

Passive air pollution control technologies represented by photocatalytic coatings have been increasingly considered the solutions to mitigate air pollution without requiring enforcement, significant capital investments or changes in human behaviour [12-16]. Photocatalytic technology, which is excited by light irradiation involving reactive radicals' oxidation process, is an ecologically and economically sustainable measure for direct air pollution control in outdoor environments [17-20]. Up to date, photocatalytic coatings have been applied to several urban microenvironments, walls and tunnels in cities all over the world, including Italy [21, 22], Germany [23], the Netherlands [24], Belgium [25], Poland [26], Span [27], China [28-30], *etc.* as listed in **Table S1** (Supporting information). The accepted products for the photocatalytic conversion of NO_x are NO_2^- and NO_3^-, which are harmless in small quantities and would be washed away by water droplets [31, 32]. Generally, photocatalysts developed in the laboratory are in powder form and are inappropriate for real-world applications [33]. However, the limitations can be overcome by coating them on the surfaces of various substrates to immobilize those powders as films. With the consideration of the practical application, the

coating products should initially possess exceptional photocatalytic performance in NO_x degradation and provide predictable health benefits. Then, the coating films generated by facile preparation methods could be adhered to different substrates without altering or affecting any existing settings. Moreover, the physicochemical properties of coating products are expected to be stable when exposed to actual roadside environments. Therefore, the development and application of photocatalytic coating for urban roadside NO_x reduction is desirable but remains challenging.

Herein, a facile method for developing photocatalytic coating products was proposed. Two types of representative construction materials as the coating substrates were investigated, considering the wide acceptance of different substrates. An artificial weather resistance test and an on-site field trial were conducted to investigate the attenuation of the photocatalytic coating. In view of the practical outcomes, the health effects were estimated and evaluated based on epidemiological statistics.

The nanosized particles are uniformly distributed in the PC-C coating film by transmission electron microscopy (TEM), as shown in **Fig. 1a**, and crystallized nanoparticles around 5–6 nm in size are observed (**Fig. 1b**), different from the TiO_2 film synthesized through traditional sol-gel methods in bulk state or nanosized greater than 50 nm [34]. The pH level of the PC-C film without adjustment is acidic due to the mild acidity H_2O_2. Considering the acidity/alkalinity of the photocatalytic film might affect its characteristics, the catalytic performance could be also altered to some extent [35]. As shown in **Fig. S5** (Supporting information), the PC-C film becomes a clear yellowish solution with desired dispersibility when the pH value is equal to or above 7. The TiO_2 film would be positively charged if the pH value is lower than the isoelectric point of 4.5–6.8 [36], which could impede the formation of TiO_2 sol and then resulting in the formation of a non-transparent colloidal solution. The crystal structures of PC-C coatings films at acid, neutral and alkaline states are displayed in **Fig. 1c**.

92 The TiO_2 anatase phase (PDF #1-526) of the PC-C coating films is well-crystallized when in
93 the acidic (pH 2–3) and neutral (pH 7) medium. When the pH level was further increases, the
94 alkaline material would break the TiO_2 crystal structure and lead to amorphous states. The X-
95 ray photoelectron spectroscopy (XPS) analysis presented in **Fig. S6a** (Supporting information)
96 revealed the presence of Ti, O, and C in the PC-C coating films synthesized in neutral medium.
97 The Ti 2p high-resolution spectrum (**Fig. S6c** in Supporting information) showed two peaks at
98 464.1 eV and 458.4 eV, which can be attributed to Ti^{4+} in TiO_2. Additionally, the O 1s spectrum
99 (**Fig. S6d** in Supporting information) exhibited two distinct peaks at 532.2 eV and 529.7 eV,
100 corresponding to surface OH and Ti-O, respectively [37].
101 Optical response comparison of TiO_2 (anatase) and PC-C coating films was investigated by
102 UV-vis DRS in **Fig. S7** (Supporting information). The adsorption edge of pristine TiO_2 is about
103 380 nm. However, the PC-C coating films is ranged from 440-480 nm. The obvious redshift of
104 PC-C coatings was considered as the peptization of H_2O_2, which modifies the crystallized size
105 of TiO_2 to around 5–6 nm, affecting the light adsorption ability of PC-C coating films.
106 Photocatalytic activity of the PC-C films with different pH levels were conducted by the
107 degradation of NO under simulated solar light irradiation in the laboratory. Material P25
108 Evonik (formerly Degussa) with the same content was used as a reference. As shown in **Fig.**
109 **1d**, the PC-C film at pH 7 showed the highest NO removal ratio (C/C_0%) that reached to
110 approximately 46.8%, which is higher than that of P25 tested at the same conditions with NO
111 removal rate at 38.8%. The photocatalytic activities of PC-C coating in acidic and alkaline
112 conditions are 31.2% and 27.3%, respectively. The photocatalytic activity of the PC-C film at
113 acid states could be affected by the incomplete sol-gel procedures, whereas the more evident
114 decrease in the alkaline environments is due to the deterioration of the TiO_2 crystallinity. It was
115 reported that amorphous TiO_2 would reduce the photocatalytic activity because of the
116 facilitated recombination of the photo-formed electrons and holes[38]. Reactive oxygen

species (ROS) of are detected in ESR when DMPO were selected as the trapping agent. As shown in **Figs. 1e and f**, the characteristic signals of both DMPO-•O_2^- and DMPO-•OH could be observed in the test samples. Notably, enhanced signals were observed in PC-C film at pH 7, indicating more ROS were generated under light irradiation for the following reactions[39].

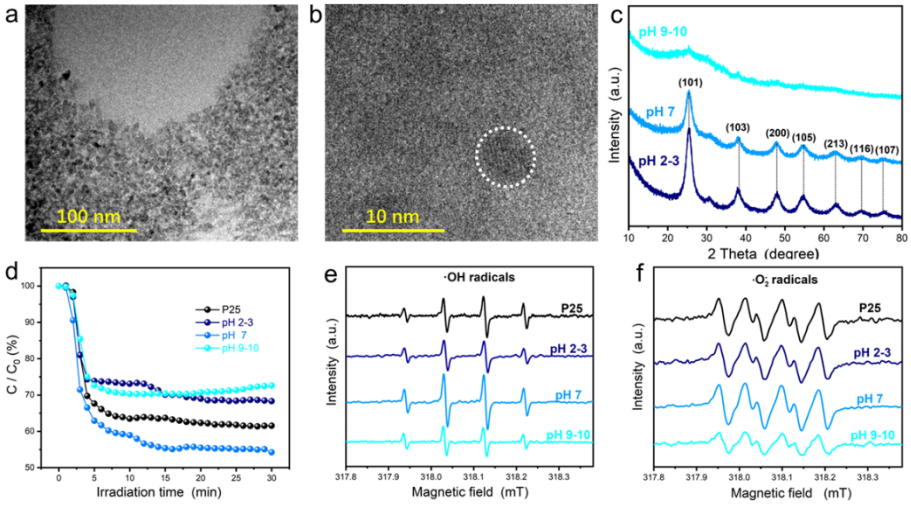

Fig. 1. TEM (a, b) of PC-C films (pH 7). XRD patterns of PC-C coating films (c) and photocatalytic activity of NO removal of PC-C coating films at different pH levels and P25 under simulated solar light (d). DMPO ESR spectra samples under simulated solar light irradiation in aqueous dispersion for DMPO-•OH (e) and in methanol dispersion for DMPO-•O_2^- (f).

In practical application, the hydrophilic surfaces could induce spread over of water droplets, where the deposited dusts and dirt are easily washed away to reach the self-cleaning effects[30]. In this study the self-cleaning capacities of the PC-C coating films were evaluated by the contact angle (CA) that was measured after Xe lamp irradiation for 3 min. As shown inn **Figs. 2a-c**, the CA values of the PC-C coating films at acid, neutral and alkaline conditions are 57.1º, < 2.0º, and 28.8º, respectively. The PC-C films at the neutral state possessed the super hydrophilicity properties, indicating the most optimal self-cleaning properties. From scanning electron microscope (SEM) in **Fig. 2d**, the side of the coated substrate is covered with

heterogeneous nanosized particles. The mapping analysis in **Fig. 2e** further demonstrate the even distribution of Ti and O, representing that substrates could be uniformly dispersed by high-pressure spraying.

Two types of representative construction materials were selected as the coating substrates for NO_x degradation. The first type was PMMA, which is a transparent thermoplastic, as a lightweight and shatter-resistant alternative to glass; the second type was concrete, which is a basic material for urban architecture. The two other commercial photocatalytic coating products labelled as PC-A and PC-B, as well as P25, labelled as PC-D, were also applied for comparisons. Detailed information on the coating products is shown in **Table S2** (Supporting information), and the as-prepared specimens are shown in **Fig. S8** (Supporting information).

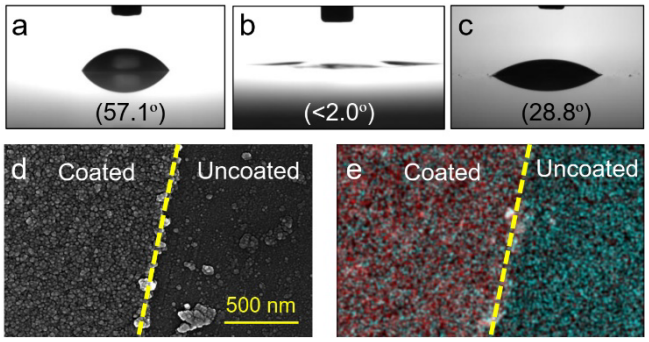

Fig. 2. CA values of PC-C films synthesized with different pH levels: pH 2-3 (a), pH 7 (b) and pH 9-10 (c). SEM image (d) and mapping analysis (e) of the high-pressure spraying coated and uncoated PC-C film on substrates, elements distribution, Ti: red, O: cyan.

The photocatalytic degradation performances of coated specimens are shown in **Figs. 3a and b**, respectively. PC-C-PMMA and PC-D-PMMA presented degradation ratios of photocatalytic NO_x removal at 5.6% and 3.8%, respectively. The corresponding NO_2 yield ratio of PC-C-PMMA was 0.5%, which was lower than 1.4% of the PC-D-PMMA. In the concrete specimen, the NO_x removal ratios followed an order of PC-C-Concrete (28.2%) > PC-D-Concrete (26.9%) > PC-A-Concrete (18.9%) > PC-B-Concrete (2.5%) ≈ blank-Concrete (2.7%). It is

worth noting that the NO_2 yield from the PC-C-Concrete is lower than that of the PC-D-Concrete specimen. In addition, the PC-C-Concrete specimen demonstrates a degradation rate of approximately 17% when NO_2 is used as the initial gas (**Fig. S9** in Supporting information), suggesting that the PC-C coating film has a direct effect on the degradation of NO_2. This finding implies that the installation of photocatalytic coating would not have any adverse impacts on air quality. **Figs. S10a and b** (Supporting information) show five-time consecutive tests of photocatalytic degradation of NO_x over PC-C-PMMA and PC-C-Concrete specimens, respectively. The two specimens present insignificant decay in photocatalytic activities, suggesting the relative stability of the PC-C over the two substrates. To illustrate the reaction mechanism of photocatalytic conversion of NO_x, the simplified photocatalytic conversion mechanism over PC-C coating is presented in **Table 1**.

Table 1

Photocatalytic reaction steps of NO_x over PC-C coating.

Reaction steps	Related reactions
Light excitation	PC-C coating+ $h\nu \rightarrow h^+ + e^-$
Adsorption	H_2O_{gas}, $O_{2gas} \rightarrow H_2O_{ads}$, O_{2ads}
	NO_{gas}, $NO_{2gas} \rightarrow NO_{ads}$, NO_{2ads}
Radicals' generation	$H_2O_{ads} + h^+ \rightarrow {}^{\bullet}OH + H^+$
	$O_{2ads} + e^- \rightarrow {}^{\bullet}O_2^-$
NO_x degradation	$NO_{gas}/NO_{2ads} + {}^{\bullet}OH \rightarrow HNO_2 + HNO_3$
	$NO_{gas}/NO_{2ads} + {}^{\bullet}O_2^- \rightarrow 2NO_2^- + NO_3^-$

From a practical perspective, the specific NO_x removal rate ($r(NO_x)$) on substrates is an important criterion in evaluation [40, 41]. **Fig. 3c** clearly shows that PC-C coatings have the highest specific NO_x removal rate on PMMA and concrete surfaces with value of 1.01 and 4.84 mg m^{-2} h^{-2}, respectively. The differences in the photocatalytic activities of the two substrates are mainly due to the physical properties of the surfaces. Restricted to the adhesive ability between the photocatalytic coating products and substrate materials, there is approximately 4 mg the coating products per PMMA test specimen, with the coating content per unit area of around 0.8 mg/cm^2. However, the coating content over the concrete specimen was

179 approximately 4.0 mg/cm^2, which had more than 300 mg coating products in total. In addition,
180 dissimilar to relatively inert PMMA, the cement-based material is chemically linked with the
181 photocatalytic coating , which renders better activity and stability [42].
182 It should be noted that NO_x^- (NO_3^- and NO_2^-) is recognised as the final products of NO_x
183 photocatalytic oxidation [43]. The NO_x-to-NO_x^- content of the specific coating was determined
184 by the detection of the washed residuals of the tested specimens (**Fig. 3d**). Even though, the
185 NO_x degradation rates of PC-A-PMMA and PC-B-PMMA specimens are relatively low, there
186 are 0.71 and 1.18 μg of NO_x^- were detected per milligrams of coating contents, respectively,
187 indicating that these coating products also have NO_x degradation effects to some extent. In
188 addition, the PC-C coating products have the highest NO_x-to-NO_x^- of 3.93 and 4.84 μg/mg on
189 the PMMA and concrete specimen, respectively. The results are constant with that of the
190 degradation activity test, where concrete specimens showed more NO_x^- accumulations than the
191 PMMA specimens.

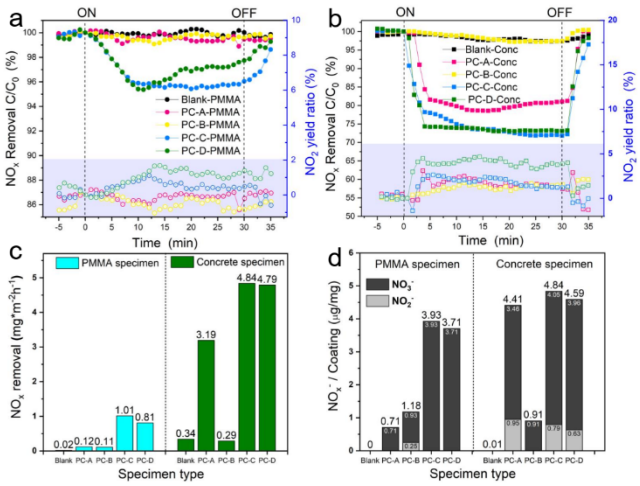

192
193 **Fig. 3**. Photocatalytic activity of NO_x removal of the coated PMMA (a) and concrete (b)
194 specimen under simulated solar light (NO as the initial gas). Specific NO_x removal rate of
195 coated specimen (c). NO_x-to-NO_2^- ratio and NO_x-to-NO_3^- ratio of the coated specimen (d).
196

Coating products will inevitably experience the attenuation effects of nature environments when applied outdoors. The artificial accelerated aging test was conducted to explore the weather resistance, as shown in **Fig. S11** (Supporting information). The comprehensive acceleration factor AFT/H/UV was calculated to be 103.8 considering the combined meteorological parameters of temperature, humidity, and ultraviolet radiation in **Table S3** (Supporting information). This finding indicates that the as-provided seven-hour aging procedure simulated approximately 100 times, i.e., 30-day of outdoor aging conditions in Hong Kong [44]. The accumulated degradation amounts of NO_x on the coated PMMA and concrete specimens that underwent artificial aging are presented in **Figs. S12a, b** and **Table S4** (Supporting information). The 30-minute NO_x degradation amounts of PC-C coating on PMMA specimen decreased from 2.51 μg to 1.25 μg (50.2%), and that on concrete specimen reduced from 17.28 μg to 14.94 μg (13.5%), respectively. Similarly, a 71.3% NO_x degradation is observed with PC-D on the PMMA, whereas only 28.5% with PC-D-Concrete. In comparison, the coating products were proven to be more stable when applied on concrete surfaces. This could be explained as the rough and porous concrete surfaces that a provide a strong binding between the coating products and the concrete surfaces [45].

The field trial involving the PC-C specimens that experience different periods of field trial would be collected back to the laboratory for NO_x degradation activity tests. The field study would directly examine the attenuation of the coated specimens exposed in the actual environments. The field trial underwent 180 days (from 25th Oct. 2021 to 23rd Apr. 2022), and the collection time are illustrated in **Tables S5 and S6** (Supporting information). Two parallel scenarios were designed in the field trials considering the role of rainfalls in outdoor environment in **Fig. S13** (Supporting information). The specimen placed with a transparent cover is denoted as scenario A, and without a transparent cover is scenario B. The field trial did not suspend during the entire period.

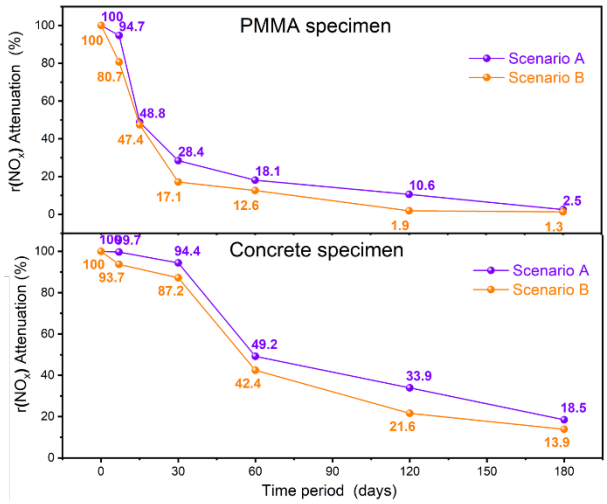

222

223 **Fig. 4**. Attenuation rate of r(NO_x) in PC-C-PMMA and PC-C-Concrete specimen over a 180-
224 day exposure time.

225

226 **Fig. 4** shows the attenuation rates of r(NO_x) of the PC-C-PMMA specimen over exposure time.
227 In scenario A with transparent shelter, the r(NO_x) of the PC-C-PMMA has a decline of 48.8%
228 from the original level after 15-day exposure, and a further drop of 18.1% after exposing for
229 60 days. Similarly, the declining trend of r(NO_x) of the specimens in scenario B attenuated
230 rapidly to 47.4% of the beginning level in the first 15 days and continues to decrease in the
231 following days. The r(NO_x) of the PC-C-PMMA specimens in both scenarios are almost zero,
232 indicating no photocatalytic effects after the 180-day exposure. Eventually, the downtrend in
233 scenario B was more distinct than that in scenario A. **Fig. 4** presents the variations of r(NO_x)
234 of the PC-C-Concrete specimens in the 180-day field trials of the two scenarios. In scenario A,
235 the r(NO_x) only decayed to 94.4% after 30-day outdoor exposure, and then decreased
236 noticeably (approximately by half) to 49.2%, experiencing 60 days of roadside environment.
237 Only 18.5% of r(NO_x) is left after completing the entire 180-day field trial. As the same
238 observation as the PC-C-PMMA, the downtrend in r(NO_x) of the PC-C-Concrete specimens is
239 more evident in scenario B than A. It remained 93.7% of the initial level after the 7-day trial,
240 and then dropped to 87.2% when the outdoor exposure time was prolonged to 30 days. The

r(NO_x) finally showed 13.9% of the original level after the entire 180-day trials. The detailed values of the degradation results are given in **Tables S7 and S8** (Supporting information). The more intense connection between PC-C coating and concrete surface was further verified in the field trial. It is noticed that all the test specimens placed in scenario A (with a transparent cover) presented higher NO_x degradation ability than the test specimens placed in scenario B (without a transparent cover) with the same exposure time, implying that the PC-C coating possesses a relatively stable NO_x degradation when away from rainfall. Although the dirt on the surface of the specimen could be splashed in scenario B, it could inevitably affect the lifetime of the coating due to the natural attenuation by rainwater.

A pre-monitoring of air quality was performed from October 3rd-31st, 2021 at the same location to act as a reference for the NO_x concentration level. Ambient NO_x (NO, NO_2) concentrations were measured continuously using an online NO_x analyzer (200E - Teledyne API), as shown in **Fig. S14** (Supporting information). The hourly averaged NO_2 concentration in the sampling month was 64.72 $\mu g/m^3$, which is much higher than AQGs with WHO and AQO with HKEPD. Furthermore, the HR of NO_2 for different ages and gender groups based on the data collected are shown in **Table 2**. The results imply that children (8–10 years old) and female adults have the relatively higher HR levels of 21.6 and 21.3, respectively. Meanwhile, male adults and infants possessed relatively lower HR of 17.5 and 17.3, respectively. In comparison with that in other studies, our average HR value obtained outside the tunnel is much higher than that in universities, tourist sites, residential areas and even factories in urban cities of China and South Korea [46, 47]. It should be noted that the HR level is positively related to NO_2 concentrations, indicating the intense adverse health outcomes for roadside residents, especially for children and women. Even though, several emission control measures have been established by the Hong Kong SAR Governments, leading to a decrease in the NO_2 concentration in recent years [48, 49]. The potential health hazard to roadside residents cannot be completely neglected.

Table 2

Somatic parameters and estimated HR of NO_2 for infants, children (8–10 years old), male adults and female adults.

Age group	BR (m^3/d)	BW (kg)	DR (μg/kg)	HR
Infants	0.8	3.0	17.3	11.5
Children (8–10 years old)	10	30.0	21.6	14.4
Adults (Male)	20	74.4	17.5	11.6
Adults (Female)	20	61.1	21.2	14.1

The Air Quality Health Impact Assessment (AirQ+ 2.1) software based on concentration–response functions established by epidemiological studies was adopted to quantify the short-term health benefits of applying photocatalytic coating technologies at the roadside environment [50]. The model was established as a 5-km^2 street canyon, and the maximum 1-hour NO_2 of hospital admissions for respiratory diseases (HARD) and expected annual number of mortality cases (MC) based on the related attributable proportion (AP) were estimated and shown in **Table S9** (Supporting information). Specifically, the average hourly NO_2 concentrations during the morning peak (07:00-10:00 LST) and evening peak (17:00-20:00 LST) on working days were 181.3 and 138.8 μg/m^3, respectively, in October 2021. With the application of the photocatalytic coating technology, it is expected to diminish the roadside NO_2 concentration to 171.1 and 130.2 μg/m^3 in the morning peak, and 131.0 and 99.6 μg/m^3 in the evening peak, with PC-C film on PMMA and concrete surface, respectively. Besides, the AP due to the exposure on the roadside NO_2 during the morning peak time was 2.5% (95%, CI:0, 6.3%) and the MC is 4.5% (95%, CI: 2.7%, 6.3%). In the evening peak time, the AP and MC are 1.9% and 3.4%, respectively. Potential health benefits of PC-C coatings applied on both PMMA and Concrete in roadside environments are expected. For example, approximately

5% and 30% reductions of HARD are found with the PC-C film on PMMA and concrete surfaces, respectively, in the morning peak hours. Therefore, the application of the PC-C coating on construction materials would effectively reduce the health expense in the roadside environment.

In summary, a facile method for the development of TiO_2-based PC-C photocatalytic coating film was prepared in this work. The nanosized PC-C coating is proven to possess a super-hydrophilicity surface and ideal NO_x degradation activity at neutral state. Both the artificial weather resistance test and on-site investigation imply that the concrete surface provides a strong bonding interaction with the coating, which is beneficial to extend the coating lifetime. Besides, the model estimates that the applications of the PC-C coating could reduce health hazards and expenses for roadside residents, especially during peak hours. This work provides a new reference for the development and practical application of photocatalytic coating for air pollution control. Even though the scale of this field trial is limited, the application of the photocatalytic coating in terms of roadside NO_x mitigation is worthwhile. A more detailed analysis regarding cost-benefits, traffic volume, and on-site monitoring in a larger scale is recommended in future studies.

Acknowledgements

This work was supported by the collaborative research project from Ove Arup & Partners Hong Kong Limited (No. P0038294), Theme-based Research Schemes (Nos. T31-603/21-N and T24-504/17-N) of Research Grants Council, Hong Kong. This research is also supported by the General Research Fund, Research Grants Council of Hong Kong Government (No. 18300920) and Dean's Research Fund (No. 04738), FLASS, EdUHK. The authors are grateful to supports from the Highway Department of Hong Kong, SAR for the field study part of this work.

References

[1] J.H. Seinfeld, S. Pandis, Atmos. Chem. Phys. 1326 (1998)33-38.

[2] T. Boningari, P.G. Smirniotis, Curr. Opin. in Chem. Eng. 13 (2016) 133-141.

[3] X. Lu, T. Yao, Y. Li, J. Fung, A. Lau, Environ. Pollut. 212 (2016) 135-146.

[4] A. Chauhan, H.M. Inskip, C.H. Linaker, et al, The Lancet, 361 (2003) 1939-1944.

[5] M. Jerrett, R.T. Burnett, B.S. Beckerman, et al., Am. J. Respir. Crit. Care Med. 188 (2013) 593-599.

[6] P. Brimblecombe, Environ. Monit. Assess. 192 (2020) 295.

[7] HKEPD, (2021). https://www.aqhi.gov.hk/api_history/english/report/files/AQR2020e_final.pdf

[8] Y. Huang, Z.H. Ling, S.C. Lee, et al., Atmos. Environ. 122 (2015) 809-818.

[9] L. Cui, X.L. Wang, K.F. Ho, et al., Atmos. Environ. 177 (2018) 64-74.

[10] HKEPD, (2021) https://www.epd.gov.hk/epd/sites/default/files/epd/english/environmentinhk/air/air_quality_objectives/files/Hong_kong_AQO.pdf

[11] WHO, (2021). https://www.who.int/publications/i/item/9789240034228

[12] D. Voordeckers, T. Lauriks, S. Denys, et al., Landscape Urban Plan, 207 (2021) 103980.

[13] A. Basso, A.P. Battisti, R. Moreira, H.. José, Environ. Technol. 41 (2020) 1568-1579.

[14] T. Maggos, J. Bartzis, M. Liakou, C. Gobin, J. Hazard. Mater. 146 (2007) 668-673.

[15] M. Gallus, V. Akylas, F. Barmpas, et al., Build Environ. 84 (2015) 125-133.

[16] M. Cai, Y. Liu, C. Wang, et al., Sep. Purif. 304 (2023) 122401-122402.

[17] Y. Nosaka, A. Nosaka, Chem. Rev. 117 (2017) 11302-11336.

[18] C. Wang, R. Yan, M. Cai, Y. Liu, S. Li, Appl. Surf. Sci. 610 (2023) 155346-155356.

[19] S. Li, M. Cai, Y. Liu, et al., Chinese J. Catal. 43 (2022) 2652-2664.

[20] S. Li, C. Wang, Y. Liu, et al., Chem. Eng.J 455 (2023) 140943.

[21] G. Guerrini, E. Peccati, Symposium on Photocatalysis, Environment and Construction Materials,(Florence/Italy), 2007, 179-186.

[22] M. Lettieri, D. Colangiuli, M. Masieri, A. Calia, Build. Environ. 147 (2019) 506-516.

[23] S. Jacobi, Modellversuch Fulda, 12 (2012) 59-66

[24] M. Ballari, H. Brouwers, J. Hazard. Mater. 254 (2013) 406-414.

[25] N. Bengtsson, M. Castellote, Mater. de Construccion. 64 (2014) 1-17.

[26] H. Witkowski, W. Jackiewiczrek, K. Chilmon, J. et al., Appl. Sci. 9 (2019) 1735-1744.

[27] J. Cordero, R. Hingorani, E. Jiménez-Relinque, et al., Sci. Total Environ. 766 (2021) 144393-144402.

[28] M. Chen, Y. Liu, J. Hazard. Mater. 174 (2010) 375-379.

[29] M. Chen, J. Chu, J. Clean. Prod. 19 (2011) 1266-1272.

[30] Y. Huang, J. Zhang, Z. Wang, et al., Sol. RRL. 4 (2020) 2000170-2000179.

[31] J. Chen, C. Poon, Build. Environ. 44 (2009) 1899-1906.

[32] L. Yang, A. Hakki, F. Wang, D.E. Macphee, Appl. Catal. B Environ. 222 (2018) 200-208.

[33] R. Zouzelka, J. Rathousky, Appl. Catal. B Environ. 217 (2017) 466-476.

[34] S.Y. Choi, M. Mamak, N. Coombs, N. Chopra, G.A. Ozin, Adv. Funct. Mater. 14 (2004) 335-344.

[35] L. Chen, J. Tian, H. Qiu, et al., Ceram. Int. 35 (2009) 3275-3280.

[36] N. Sasirekha, B. Rajesh, Y. Chen, Thin Solid Films, 518 (2009) 43-48.

[37] Y. Chen, W. Li, J. Wang, et al, Appl. Catal. B Environ. 191 (2016) 94-105.

[38] B. Neppolian, H. Jung, H. Choi, J. Adv. Oxid. Technol. 10 (2007) 369-374.

[39] A.H. Mamaghani, F. Haghighat, C.S. Lee, Chemosphere, 219 (2019) 804-825.

[40] M.Z. Guo, C. Poon, Build. Environ. 70 (2013) 102-109.

[41] P. Munafò, G.B. Goffredo, E. Quagliarini, B. Materials, Constr Build Mater. 84 (2015) 201-218.

[42] M.Z. Guo, A. M. Ramirez, C.S. Poon, J. Clean. Prod. 112 (2016) 3583-3588.

[43] X.W. Li, W.D. Zhang, J.Y. Li, et al., Appl. Catal. B Environ. 241 (2019) 187-195.

[44] U. Berardi, R.H. Nosrati, Energy, 147 (2018) 1188-1202.

[45] M.Z. Guo, T.C. Ling, C.S. Poon, Environ. Pollut. 273 (2021) 116510-116519.

[46] Z. Liu, Q. Guan, H. Luo, et al., Atmos. Environ. 213 (2019) 515-525.

[47] H.T. Nguyen, K.H. Kim, C. Park, Atmos. Environ. 106 (2015) 347-357.

[48] X. Lyu, H. Guo, I.J. Simpson, et al., Atmos. Chem. Phys. 16 (2016) 6609-6626.

[49] D. Yao, X. Lyu, F. Murray, et al., Sci. Total Environ. 648 (2019) 830-838.

[50] WHO, (2018). https://www.who.int/europe/tools-and-toolkits/airq---software-tool-for-health-risk-assessment-of-air-pollution.

Supplementary material

Supporting text associated with this article can be found in this section, including preparation of specimens, characterization methods, evaluation systems of photocatalytic activity test, health risk method, field test investigations photos of prepared PMMA, Concrete specimen, and the coating procedure, XPS spectra analysis, UV-vis DRC of PC-C coating at different pH level, specimens undergo weather resistance test. Diagram of photocatalytic degradation system, location of field trial, cycling runs of photocatalytic removal rate of NO_x over the PC-C-PMMA and PC-C-Concrete specimen. The NO and NO_2 concentration collected from 03 October 2021 to 31 October 2021. The detailed information of selected photocatalytic coating products. NO_x degradation activity test of PMMA and Concrete specimens after irradiation resistance test, PMMA and concrete specimen collection schedule, NO_x degradation activity test of PC-C-PMMA and PC-C-Concrete after different period of field trial. Results of estimated maximum one-hour NO_2 of HARD and expected annual number of cause-specific mortality MC and related attributable proportion (AP)

Supplementary contents

Preparation of specimens

The PMMA specimen prepared with dimension of 100 mm (L) x 50 mm (W) x 15 mm (H). The concrete specimens were prepared in a round shape with a diameter of 100 mm (D). The size of the specimen was determined with reference to ISO 22197-1.[1] High-pressure spraying was performed for uniform dispersion of the photocatalytic coating products on the PMMA and concrete specimen. The pressure of the air compressor unit was 10 kPa, and the distance of the nozzle from the substrate surface was 0.5 – 1.0 m to ensure adequate atomization of the liquid photocatalyst. A 10-time repeated unified sweeping method was used for spraying the coating products on the specimens. The coating volume on each specimen during the spraying process was controlled as 10 ± 2 mL. The photos of the prepared specimen and the coating procedure are shown in Fig. S1.

Characterization methods

The crystal phases of the sample were analyzed by X-ray diffraction (XRD) with Cu Kα radiation (model D/max RA, Rigaku Co., Japan). Scanning electron microscopy (SEM; model JSM-6490, JEOL, Japan) and transmission electron microscopy (TEM; JEM-2010, Japan) were used to characterize the morphology and structure of the obtained products. X-ray photoelectron spectroscopy (XPS) with Al Kα X-rays (hm = 1486.6 eV) radiation operated at 150 W (Escalab 250Xi) was used to investigate the surface properties. All binding energies were calibrated by C 1s at 284.8 eV as a reference. A Varian Cary 100 Scan UV-visible system equipped with a Labsphere diffuse reflectance accessory was used to obtain the reflectance spectra of the catalysts over a range of 200 to 800 nm. The contact angle (CA) (θ) was measured according to ISO 15989:2004 on a CA goniometer system (SL200KS, USA KINO Industry Co., Ltd.) to evaluate the self-cleaning performance of the film (ISO 15989: 2004).[2] The concentrations of NO_2^- and NO_3^- on the surface of the photocatalysts were measured by ion chromatography (930 Compact IC Flex, Metrohm in Swiss) under the following chromatographic conditions: eluent (3.6 mmol/L Na_2CO_3), Metrosep A Supp 7 - 250/4.0 column, injection volume (250 µL), flow rate (0.7 mL/min), column

temperature (318.15 K) and automatic regeneration suppression system (100 mmol/L H_2SO_4); they were detected by an electrical conductivity detector. The standard curve of NO_2^- and NO_3^- of High-Performance IC was provided in Fig. S2. Reactive radical formation was detected through electron spin resonance spectroscopy (ESR, ER200-SRC, Bruker, Germany) using 5, 5-dimethyl-1-pyrroline-N-oxide (DMPO) as spin-trap reagent under visible light irradiation. 0.05g. sample was dispersed into 25 mmol/L DMPO solution with a 50 mL aqueous dispersion for DMPO-•OH or 50 mL methanol dispersion for DMPO-•O_2^-, respectively. A 300 W Xe arc lamp (PLS-SXE 300, Beijing) was used as light source.

Evaluation of the photocatalytic degradation of NO_x

The photocatalytic activity test of the coating products and specimen in terms of NO_x ($NO + NO_2$) degradation was conducted in a continuous-flow testing system (Fig. S3), which was established according to available ISO standards (ISO 22197-1 and ISO 22197-4) and our previous studies[3]. The testing system consists of a 4.5-L reactor with irradiation source, a NO_x analyzer (200E - Teledyne API) and one gas synthesis system including standard gas cylinder provided by Scientific Gas Engineering Co., Ltd., zero air generator and mass flow controller. In the typical testing, the test specimen was initially placed inside the reactor without a light source, and 400 ppb NO_x gas (NO mainly) with controlled flow rate at 3 L/min was introduced to the reactor until the effluent concentration reached a stable state the same as the influent concentration. Then, the simulated solar light source was added over the reactor for a 30-minute reaction. The effluent concentrations of the reactor were recorded, and the gas stream was continuously supplied during this period. The degradation rate of NO_x (η_{NOx}) from the test specimens is calculated by equation (Eq. 1), as follows:

$$\eta_{\mathrm{NOx}} = \frac{C_0 - C_t}{C_0} \times 100 \qquad \text{(Eq.1)}$$

where C_t is the outlet concentration of NO_x after the reaction, for reaction time *t*; C_0 represents the initial inlet concentration.

The amount of NO_x removal Q_{NOx} is calculated by equation (Eq. 2), and the specific NO_x removal rate (r_{nox}) is calculated by (Eq. 3), following JIS R 1701-1.[4]

$$Q_{NOx} = \frac{f}{22.4}\int (C_0 - C_t)_{dt} \quad \text{(Eq.2)}$$

$$r_{(NOx)} = \frac{Q_{NOx} \times MW_{NOx} \times 10^3}{t \times S} \quad \text{(Eq.3)}$$

where *f* refers to the flow rate converted into standard state; MW is the molecular weight (NO_x is calculated as NO_2); *S* is the surface area of the specimen.

2Outdoor photocatalytic degradation experiments

A 180-day field trial was conducted to investigate the attenuation of photocatalytic coating exposure in the actual traffic environment from October 25th 2021 to April 23rd 2022. The field trial was conducted at the conjunction of Yuk Choi Road and Hong Chong Road in Hong Kong. The proposed field trial site was approximately 400 m away from the entrance of the cross-harbour tunnel (Fig. S4), which is a typical traffic-related location and representative of the actual vehicular emissions presented represent the actual vehicular emission condition of the roadside environment.

Health risk (HR) assessment

The average dose rate and personal HR were evaluated by Eq. 4, as follows:

$$HR = \frac{DR}{LOAEL(pollutant)} \quad \text{(Eq.4)}$$

where *LOAEL(pollutant)* indicates the lowest observed adverse effect level of pollutants, and the *LOAEL(NO_2)* is 1.42 ug/kg.[5] *DR* indicates the dose rate (μg/kg) of pollutants, which was determined by equation as follows.

$$DR = \frac{BR}{BW}\int_0^{24} C_{(t)} Of_{(t)} dt \quad \text{(Eq.5)}$$

where *BR* is the breathing rate (m^3/day); *BW* refers to body weight (kg); *C(t)* is the concentration of pollutant at *t*, and *Of(t)* is assumed as 1 for any time *t* (i.e., the probability of 1 to occupy the monitoring site at any time). [6, 7]

AirQ+ (v2.1.1) software developed by WHO was adopted to evaluate the HR of short-term effects of atmospheric pollutants in a specific area. The estimation was based on the attributable proportion (AP) to specific air pollutant (NO_2) exposure for a certain time, and the AP can be estimated using Eq. 6, considering multi-age compositions exposed to different pollutants, as follows:[8, 9]

$$AP = \frac{\sum(RR_{(c)} - 1) \times P_{(c)}}{\sum RR_{(c)} \times P_{(c)}} \quad \text{(Eq. 6)}$$

where *RR(c)* is the relative risk for the health endpoint in the category of exposure (*c*), and *P(c)* is the proportion of the population in the category of exposure (*c*). This formula can be simplified to Eq. 7 with one population group, as follows:[10]

$$AP=(RR - 1) /RR \quad \text{(Eq. 7)}$$

RR was evaluated by the following equation:

$$RR=e^{[\beta \times (C-C_0)]} \quad \text{(Eq. 8)}$$

where β is the regression coefficient derived from meta-analysis; per 10 μg/m^3 increases in gaseous pollutants NO_2, the total mortality risk increased by 1.30%.[11] *C* is the concentration of pollution, and C_0 is the pollutant concentration of the National Standard II. The expected number of mortality cases (MC) due to air pollution was calculated using Eq. 9, as follows:[10]

$$MC = E \times B \times P \quad \text{(Eq.9)}$$

where *E* represents the expected number of deaths due to air pollution, *B* represents the mortality rate, and *P* represents the relevant exposed population.

Figures

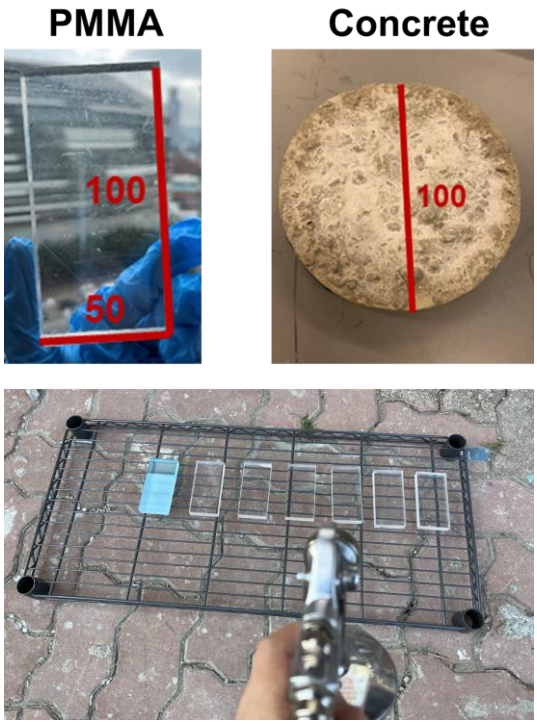

Fig. S1 Photos of prepared PMMA, Concrete specimen, and the coating procedure.

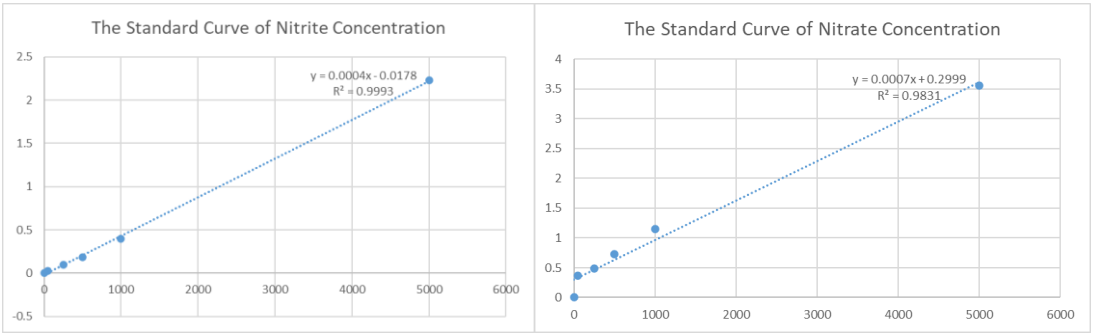

Fig S2. The standard curve of NO_2^- and NO_3^- of High-Performance Ion Chromatography

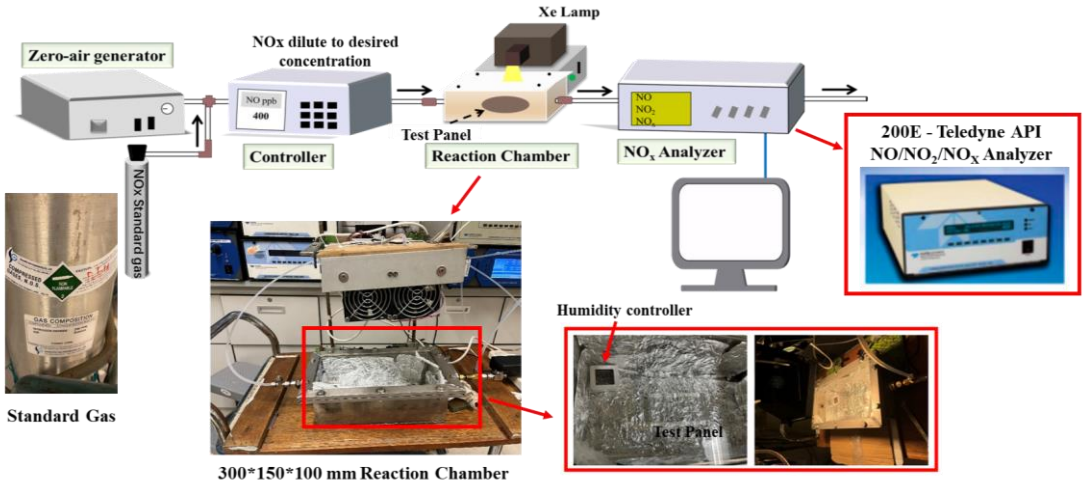

Fig. S3 The NO_x photocatalytic degradation system

There were similar systems for NO_x photocatalytic degradation from other groups that from all over the world for both laboratory and field tests. [12-17]

Fig. S4 The location of field trial. The location of field trials is the conjunction of Yuk Choi Road and Hong Chong Road in Hong Kong.

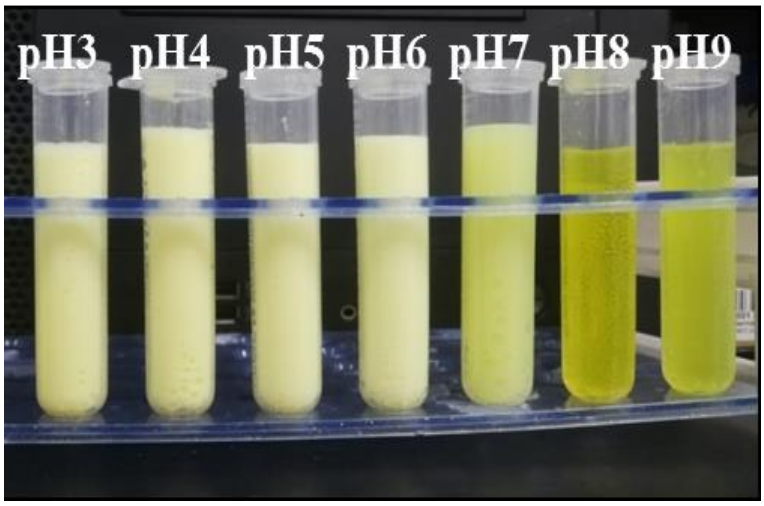

Fig. S5. The photo of PC-C photocatalytic films synthesized at pH level from 3-10.

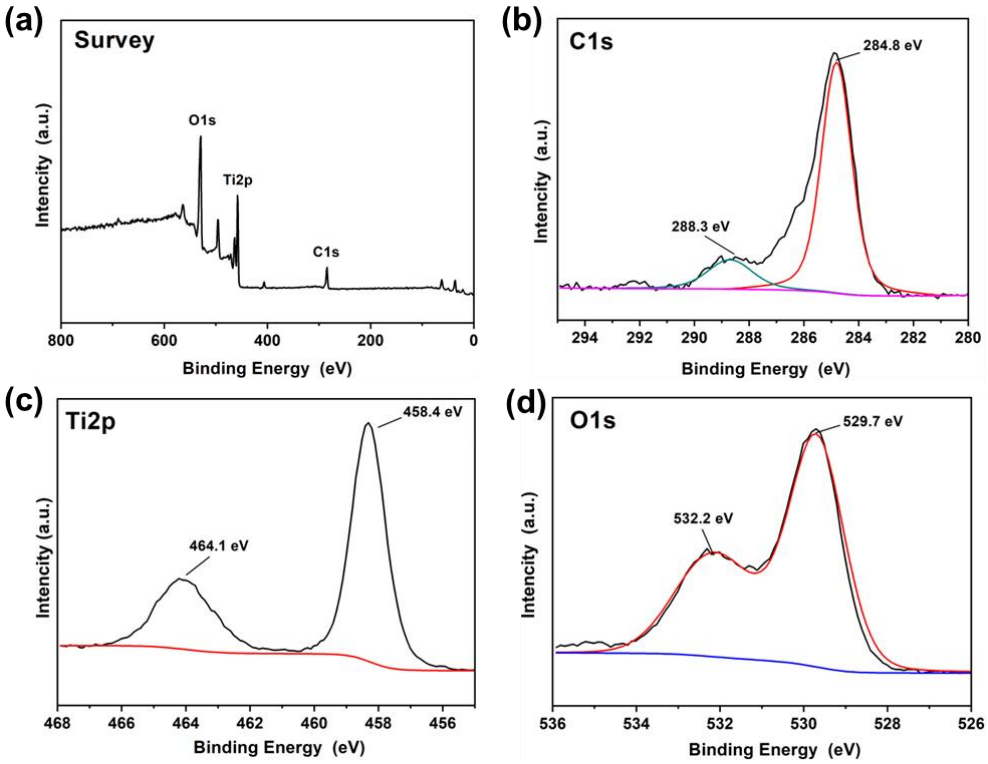

Fig.S6. XPS survey, C1s, Ti2p, and O1s spectra of PC-C film when pH=7

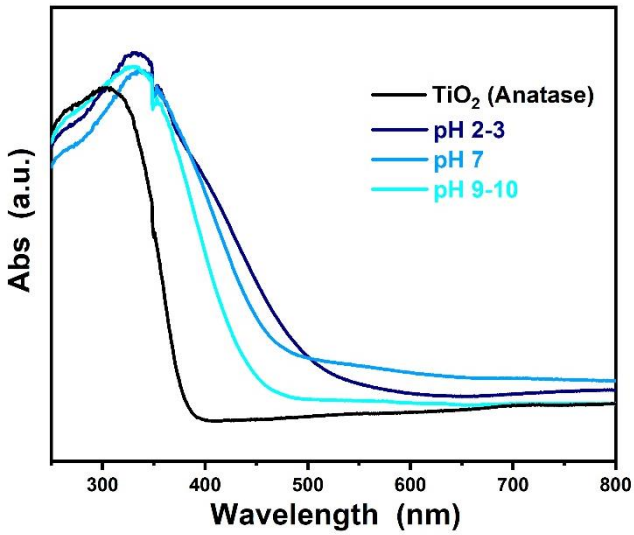

Fig. S7. The UV-vis DRS spectra of PC-C coating films synthesized at different pH levels.

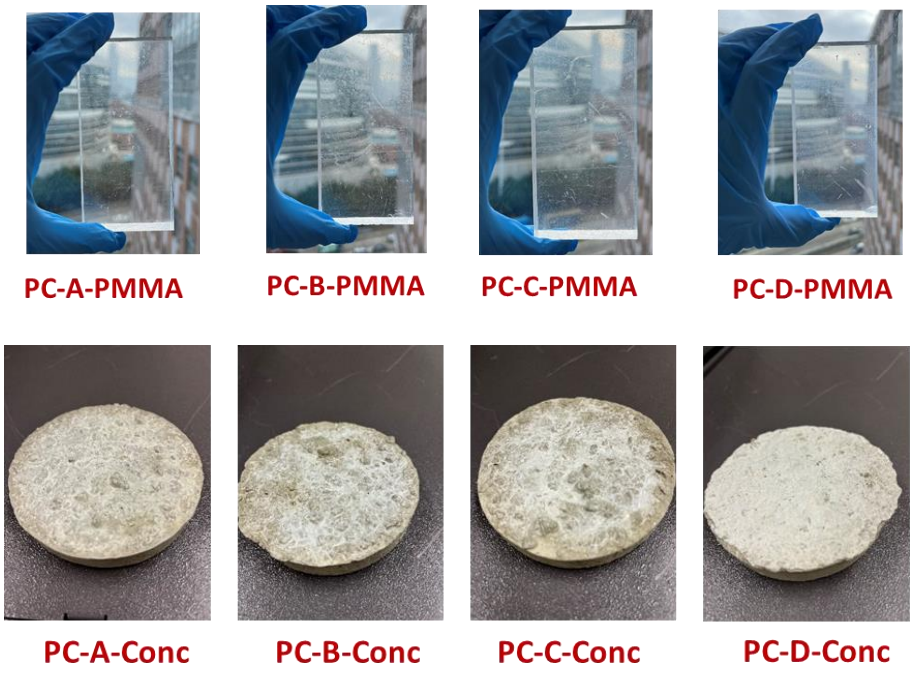

Fig. S8. The photos of as prepared PMMA and Concrete specimens

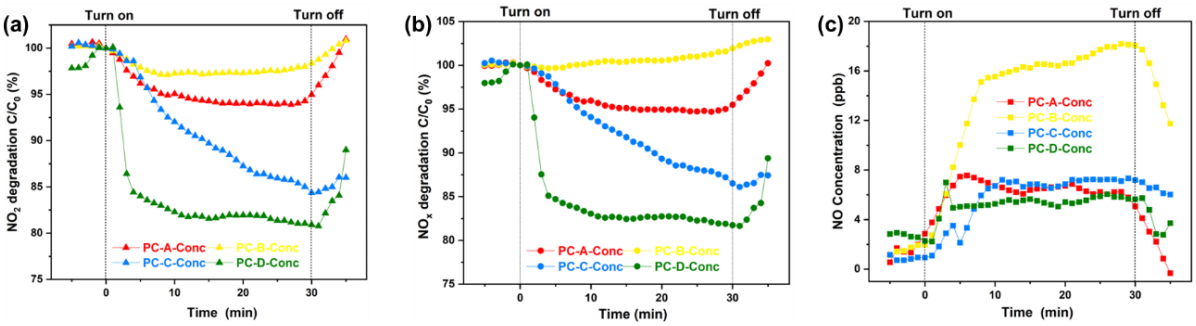

Fig. S9. Photocatalytic activity of NO_x (a) and NO_2 (b) removal and corresponding NO generation (c) of the coated concrete specimen under simulated solar light when NO_2 as the initial gas.

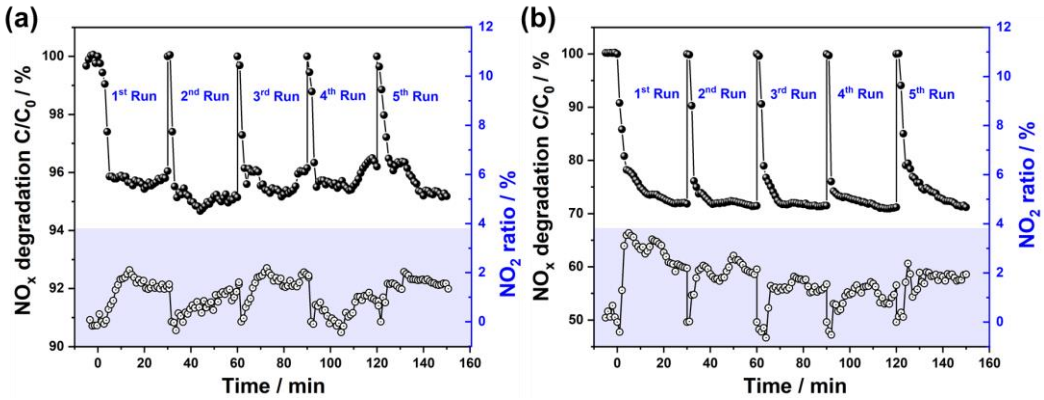

Fig. S10 The 5-times cycling runs of photocatalytic removal rate of NO_x over the PC-C-PMMA (a) and PC-C-Concrete specimen (b).

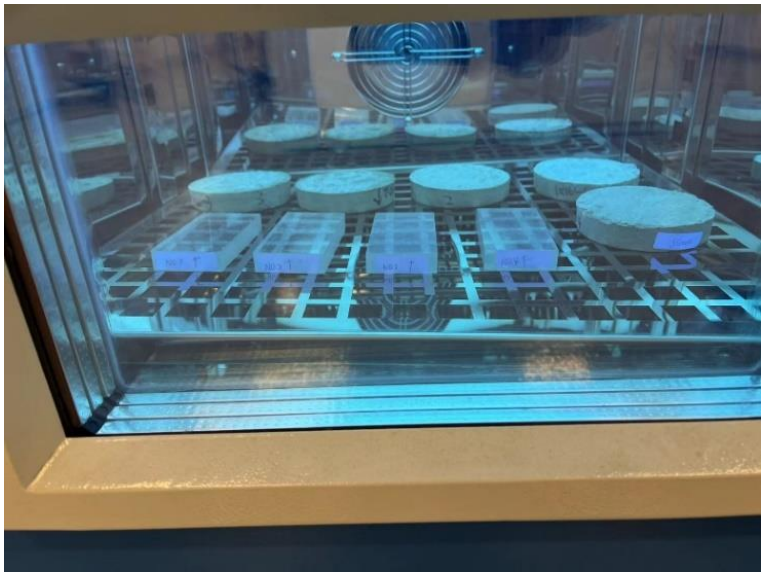

Fig. S11 The specimens undergo weather resistance test.

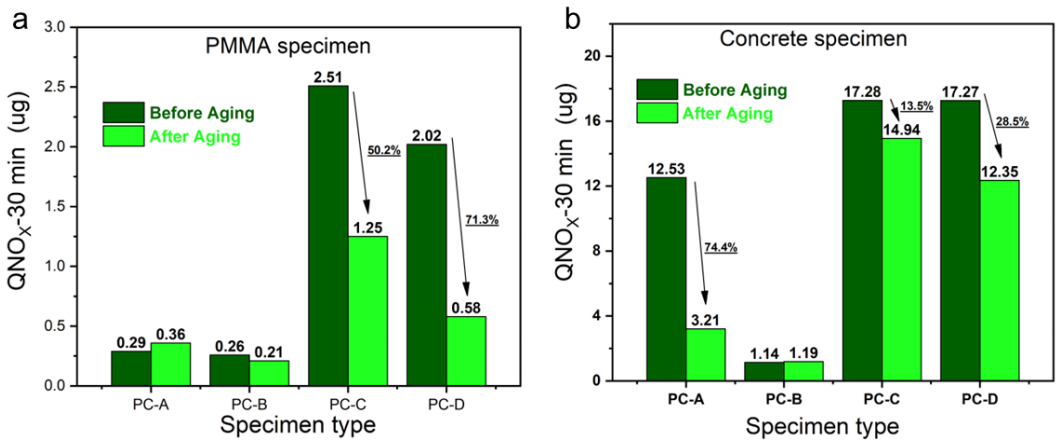

Fig. S12 Degradation amounts of NO_x after 30-minute degradation test before and after aging on PMMA (a) and concrete specimen (b)

Fig. S13. Photos of set-up for Scenario A with a transparent cover (a) and Scenario B without a transparent cover (b) of field trials.

Two parallel scenarios were designed in the field trials considering the role of rainfalls in outdoor environment. Specifically, the specimens exposed to the roadside environment with a transparent cover is denoted as scenario A (Fig. S13a). The transparent shelter in scenario A would not seal the interspace, and the air was able to access the surfaces of the test specimens. The specimens without transparent cover and totally exposed to the environment is designated as scenario B (Fig. S13b). The field trial did not suspend during the entire period.

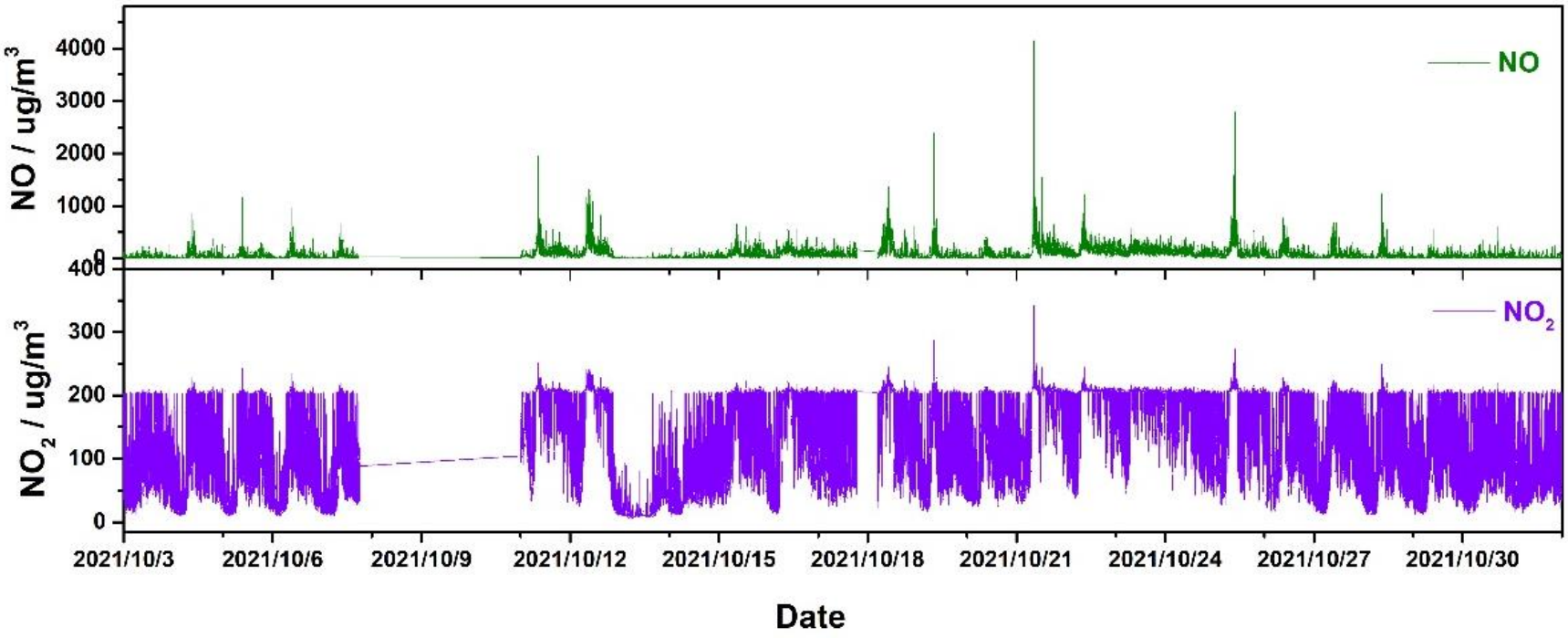

Fig. S14 The NO and NO_2 concentration collected from 03 October 2021 to 31 October 2021 at the same location of field trial.

Tables

Table S1 Overview on previous real-scale studies of photocatalytic application in the real world

Location	Application	Materials	Target pollutants, degradation rate (%)	Ref.
Bergamo (Italy)	Road and sidewalk	Photocatalytic concrete paving blocks	NO_x, 20-56	[18]
Tsitsihar (China)	Highway	Asphalt coated with photocatalytic spray solution	NO_2, 6-12	[19]
Tsitsihar (China)	Highway	Concrete coated with photocatalytic spray solution	NO_2, 12-24	[20]
Fulda (Germany)	Sidewalk	Pavement blocks with photocatalytic coating	NO, 0-17	[21]
Hengelo (Netherlands)	Road	Concrete paving blocks with photocatalytic layer (5 mm) + sprayed suspension coating	NO_x, 0-45	[22]
Chesterfield (USA)	Highway	Concrete with photocatalyst in bulk	NO_x,0	[23]
Antwerp (Belgium)	Parking lane	Concrete paving blocks with photocatalytic wearing layer (8 mm)	NO_x,16-37	[24]
Zielona Gora (Poland)	Bicycle lane	Concrete paving blocks with TiO_2-based top layer (5 mm)	NO_x, 5-45	[25]
Madrid city (Span)	Road and Pavements	Coating applied on both road (asphalt) and pavement tiles (concrete) surface	NO_x, 2.4-10.1	[26]

Bari (Italy)	Compact limestone	TiO_2 NPs to cement mixes, including anatase (42%), rutile phases (33%), and brookite (25%)	Rhodamine B, 70%	[27]
Xi'an, (China)	Road and Pavements	Direct spraying g-C_3N_4/TiO_2 Composite Film	NO, 57.3%	[14]

Table S2 The detailed information of selected photocatalytic coating products

Coating Item	PC-A	PC-B	PC-C	PC-D
Supplier	Healthy Giant Limited (Imported from Germany) https://en.healthygiant.hk/	Jinan Tian kong Zhan nan Environmental Service Co. http://www.jntkzl.com/	Synthesized in this work	Analytical Reagent[28] produced by Degussa (Evonik, German) and supplied by Oriental Chemicals & Lab. Supplies Ltd.
Density	1 g/mL	1 g/mL	1 g/mL	1 g/mL
Photos of the selected coating products				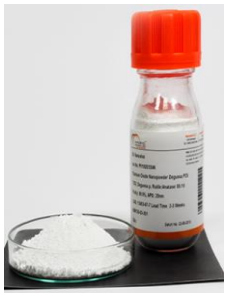

Table S3 Test conditions of weather resistance experiment

Conditions	Temperature / K	Humidity / %	Annual UV amount / kJ/m^2	Total Test Time / h
Actual conditions*	T_A = 294.15	RH_A= 77	149,600	
Simulated aging conditions	T_E = 318.15	RH_E= 90	1198,368	7 h
Aging factor (AF)	AF_T = 8.58	AF_H = 1.51	AF_{uv}=8.01	

$$AF_{T/H/UV} = AF_T \times AF_H \times AF_{UV} = 103.8$$

*The annual average air temperature is 21 °C/294.15 K in Hong Kong, the relative humidity is 77%, and the annual average total UV radiation in the Northern Hemisphere city is 149.6 MJ/m^2. [29, 30]

Table S4 NO_x degradation activity test of PMMA and Concrete specimens after irradiation resistance test

Test Conditions	Sample No.	$\eta(NO_x)$ / %	$\eta(NO)$ / %	$\eta(NO_2)$ / %
	PC-A-PMMA	0	0	0
	PC-B-PMMA	0	0	0
Inlet gas concentration:	PC-C-PMMA	2.2	1.9	0.3
400 ppb NO	PC-D-PMMA	0.6	1.2	-0.6
Flow rate: 2.7-3 L/min	PC-A-Concrete	4.5	4.4	0.1
Test pic: 1 pic	PC-B-Concrete	2.4	3	-0.6
	PC-C-Concrete	23.5	24.4	-0.9
	PC-D-Concrete	19.6	21.8	-2.2

Table S5 PMMA specimen collection schedule for degradation activity test in the field trial

Collection Time	Scenario A	Scenario B
0	PMMA-0-A	PMMA-0-B
7 days	PMMA-7d-A	PMMA-7d-B
15 Days	PMMA-15d-A	PMMA-15d-B
30 Days	PMMA-30d-A	PMMA-30d-B
60 Days	PMMA-60d-A	PMMA-60d-B
120 Days	PMMA-120d-A	PMMA-120d-B
180 Days	PMMA-180d-A	PMMA-180d-B
Blank* (after 180 days)	PMMA-b-A	PMMA-b-B
Subtotal specimens collected	9 pics	9 pics
Total PMMA specimen collected		18 pics

*Black specimen refers to PMMA specimen placed at the same environment of tested specimen but without coating

Table S6 Concrete specimen collection schedule for degradation activity test in the field trial

Collection Time	Scenario A	Scenario B
0	Concrete-0-A	Concrete-0-B
7 days	Concrete-7d-A	Concrete-7d-B
30 days	Concrete-30d-A	Concrete-30d-B
60 days	Concrete-60d-A	Concrete-60d-B
120 days	Concrete-120d-A	Concrete-120d-B
180 days	Concrete-180d-A	Concrete-180d-B
Blank* (after 180 days)	Concrete -b-A	Concrete -b-B
Subtotal specimens collected	7 pics	7 pics
Total Concrete specimen collected		14 pics

*Black specimen refers to concrete specimen placed at the same environment of tested specimen but without coating

Table S7 NO_x degradation activity test of PC-C-PMMA after different period of field trial in two scenarios (scenario A with transparent cover and scenario B without transparent cover)

Test Specimen	Test specimen collection date	Field trial period	Test scenario	$\eta(NO_x)$ /%	$\eta(NO)$ / %	$\eta(NO_2)$ / %
PC-C-PMMA Specimen	25 Oct. 2021	0	PMMA-0-A	5.4	5.1	0.3
			PMMA-0-B	4.1	4	0.1
	01 Nov. 2021	7d.	PMMA-7d-A	4.5	5.5	-1
			PMMA-7d-B	4.7	5	-0.3
	09 Nov. 2021	15 d.	PMMA-15d-A	3.5	3.9	-0.4
			PMMA-15d-B	4.7	4.5	0.2
	24 Nov. 2021	30 d.	PMMA-30d-A	3.5	3.6	-0.1
			PMMA-30d-B	3.2	3.3	-0.1
	24 Dec. 2021	60 d.	PMMA-60d-A	1.3	3.2	-1.9
			PMMA-60d-B	2.9	4.5	-1.6
	22 Feb. 2022	120 d.	PMMA-120d-A	0.8	1.8	-1
			PMMA-120d-B	0.4	0.9	-0.5
	23 Apr. 2022	180 d.	PMMA-180d-A	-0.4	1.1	-1.5
			PMMA-180d-B	0.4	0.5	-0.1
	23 Apr. 2022	180 d.	PMMA-b-A	0.3	0.4	-0.1
			PMMA-b-B	-0.2	0.6	-0.8

Fig. S8 NO_x and NO degradation profile PC-C-Concrete specimens after different period of field trial in two scenarios (scenario A with transparent cover and scenario B without transparent cover)

Test Specimen	Test specimen collection date	Field trail period	Test scenario	$\eta(NO_x)$ /%	$\eta(NO)$ / %	$\eta(NO_2)$ / %
PC-C-Concrete Specimen	25 Oct. 2021	0 days	Concrete-0-A	26.4	29.5	-3.1
			Concrete-0-B	25.8	26.8	-1
	01 Nov. 2021	7 days	Concrete-7d-A	26.3	24.1	2.2
			Concrete-7d-B	24.2	24.9	-0.7
	24 Nov. 2021	30 days	Concrete-30d-A	24.9	25.7	-0.8
			Concrete-30d-B	22.5	23.7	-1.2
	24 Dec. 2021	60 days	Concrete-60d-A	13.0	11.0	2.0
			Concrete-60d-B	10.9	11.0	0.1
	22 Feb. 2022	120 days	Concrete-120d-A	8.9	9.1	-0.2
			Concrete-120d-B	5.6	8.8	-3.2
	23 Apr. 2022	180 days	Concrete-180d-A	4.9	7.4	-2.5
			Concrete-180d-B	3.5	5.0	-1.5
	23 Apr. 2022	180 days	Concrete -b-A	2.4	3.7	-1.3
			Concrete -b-B	1.9	4.6	-2.7

Table S9 Estimated maximum one-hour NO_2 of HARD and expected annual number of cause-specific mortality MC and related attributable proportion (AP)

Health indicators		Morning Peak			Evening Peak		
		Ambient	PMMA	Concrete	Ambient	PMMA	Concrete
NO_2 concentration / ug/m^3		181.3	171.1	130.2	138.8	131.0	99.6
HARD	AP / %	2.5 (0–6.3)	2.4 (0–5.9)	1.8 (0–4.5)	1.9 (0–4.8)	1.8 (0–4.5)	1.3 (0–3.3)
	Person	7.7 (0–19.1)	7.2 (0–18.0)	5.4 (0–13.5)	5.8 (0–14.5)	5.4 (0–13.6)	4.0 (0–10.1)
MC	AP / %	4.5 (2.7–6.3)	4.3 (2.5–5.9)	3.2 (1.9–4.5)	3.4 (2.0–4.8)	3.2 (1.9–4.5)	2.4 (1.4–3.3)
	Person	13.7 (8.2–19.1)	12.9 (7.7–18.0)	9.7 (5.8–13.5)	10.3 (6.2–14.5)	9.7 (5.8–13.6)	7.2 (4.3–10.1)

Reference

[1] A. Mills, R. Andrews, R. Han, C. O. Rourke, S. Hodgen, J. Photochem. Photobiol. A. 400 (2020) 112734.

[2] Y. Huang, P. Wang, Z. Wang, et al., Appl. Catal. B Environ. 240 (2019) 122-131.

[3] Z. Wang, Y. Huang, M. Chen, et al., ACS Appl. Mater. Inter. 11 (2019) 10651-10662.

[4] R JIS, Japanese Standards Association, (2004). https://webdesk.jsa.or.jp/preview/pre_jis_r_01701_001_000_2016_e_ed10_i4.pdf

[5] M. Neuberger, H. Moshammer, M. Kundi, Atmos. Environ. 36 (2002) 1733-1736.

[6] R. Usmani, A. Saeed, A. Abdullahi, et al., Air Qual. Atmos. Hlth. 13 (2020) 1093-1118.

[7] M. Stranger, S. Vermaak, R. Van Grieken, Sci. Total Environ. 407 (2009) 1182-1192.

[8] M. Miri, Z. Derakhshan, A. Allahabadi, et al., Environ. Res. 151 (2016) 451-457.

[9] M. Ansari, M.H. Ehrampoush, Environ. Res. 170 (2019) 141-150.

[10] B. Ostro, World Health Organization, 5(2004)6-17.

[11] Y. Shang, Z. Sun, J. Cao, et al., Environ. Int. 54 (2013) 100-111.

[12] C.S. Poon, E. Cheung, Constr Build Mater. 21 (2007) 1746-1753.

[13] M.Z. Guo, C.S. Poon, Cem. Concr. Compos. 90 (2018) 42-49.

[14] Y. Huang, J. Zhang, Z. Wang, et al., Sol. RRL. 4 (2020) 2000170-2000179.

[15] A. Folli, M. Strøm, T.P. Madsen, et al., Atmos. Environ. 107 (2015) 44-51.

[16] Q.L. Yu, Y. Hendrix, S. Lorencik, H. Brouwers, Build. Environ. 142 (2018) 70-82.

[17] G.L. Guerrini, Constr. Build. Mater. 27 (2012) 165-175.

[18] G. Guerrini, E. Peccati, Symposium on Photocatalysis, Environment and Construction Materials,(Florence/Italy), 2007, 179-186.

[19] M. Chen, Y. Liu, J. Hazard. Mater. 174 (2010) 375-379.

[20] M. Chen, J. Chu, J. Clean. Prod. 19 (2011) 1266-1272.

[21] S. Jacobi, Modellversuch Fulda, 12 (2012). 59-66

[22] M. Ballari, H. Brouwers, J. Hazard. Mater. 254 (2013) 406-414.

[23] J.K. Sikkema, Dordt University (2013).

[24] N. Bengtsson, M. Castellote, Mater. de Construccion. 64 (2014) 1-17.

[25] H. Witkowski, W. J. Rek, K. Chilmon, et al., Appl. Sci. 9 (2019) 1735.

[26] J. Cordero, R. Hingorani, E. J. Relinque, et al., Sci. Total Environ. 766 (2021) 144393-144402.

[27] M. Lettieri, D. Colangiuli, M. Masieri, A. Calia, Build. Environ. 147 (2019) 506-516.

[28] A.K. Datye, G. Riegel, J. Bolton, M. Huang, M. Prairie, J. Solid State Chem. 115 (1995) 236-239.

[29] N. Xie, H. Li, H. Zhang, et al., Energ. Mat. Sol. C. 215 (2020) 110698-110707.

[30] H.K. Observatory, Climate of Hong Kong. https://www.hko.gov.hk/en/cis/climahk.htm